Materials Science in Semiconductor Processing 167 (2023) 107786

Contents lists available at ScienceDirect

Materials Science in Semiconductor Processing

journal homepage: www.elsevier.com/locate/mssp

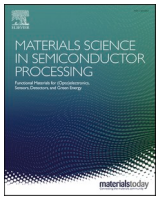

Lateral photovoltaic effect in silicon-based hybrid structures under external magnetic field

I.A. Bondarev [a,b,*], M.V. Rautskii [a], N.V. Volkov [a], A.V. Lukyanenko [a,c], I.A. Yakovlev [a], S.N. Varnakov [a], A.S. Tarasov [a,c,**]

[a] Kirensky Institute of Physics, Federal Research Center KSC SB RAS, Krasnoyarsk, 660036, Russia
[b] Federal Research Center "Krasnoyarsk Scientific Center of the Siberian Branch of the Russian Academy of Sciences", Krasnoyarsk, 660036, Russia
[c] Siberian Federal University, Institute of Engineering Physics and Radio Electronics, Krasnoyarsk, 660041, Russia

ARTICLE INFO

Keywords:
Lateral photovoltaic effect
MIS structures
Interface states
Schottky field

ABSTRACT

Charge transport in semiconductor devices is highly sensitive to light, which opens up wide application prospects. The lateral photovoltaic effect (LPE) is widely used in position sensitive detectors due to its high sensitivity to the light spot position. We report on the features of the LPE in silicon-based metal/insulator/semiconductor structures at helium temperatures. To investigate the LPE, Fe/SiO_2/p-Si and Mn/SiO_2/n-Si structures have been fabricated by molecular beam epitaxy. It has been found by studying the lateral photovoltage that the SiO_2/Si interface plays a significant role in transport of photogenerated carriers, mainly via the interface states, which induce electron capture/emission processes at certain temperatures. The value of the photovoltage is likely affected not only by the metallic film thickness, but also by the substrate conductivity type and Schottky barrier. The effect of the magnetic field on the LPE is driven by two mechanisms. The first one is the well-known action of the Lorentz force on photogenerated carriers and the second one is shifting of the interface state energy levels. Basically, the magnetic field suppresses the contribution of the interface states to the LPE, which suggests that the interface-induced transport can be controlled magnetically.

1. Introduction

Magnetotransport phenomena in multilayered nanostructures have attracted considerable scientific interest since the discovery of the giant magnetoresistance effect (GMR) [1]. Metal/insulator/semiconductor (MIS) structures have been in the special focus due to compatibility with CMOS and SOI technology. Magnetic control over the electronic properties has allowed MIS structures to find various applications in modern electronics, in particular, in magnetic field sensors and MRAM elements. In recent years, a number of studies have been devoted to the lateral photovoltaic effect (LPE) in MIS structures [2–5]. The lateral photovoltaic effect, which was first discovered by Schottky [6] and expanded upon by Wallmark in floating Ge *p–n* junctions [7], is widely utilized in position sensitive detectors due to its high sensitivity to the light spot position [8–10]. The implementation of the LPE in MIS structures has opened ways to the further development of optical sensors and solar cells. It has been shown that the LPE is sensitive to external magnetic fields [11–15]. Wang et al. studied the LPE in silicon-based structures with soft ferromagnetic (FM) materials and found that the lateral photovoltage (LPV) in both Si and FM layer was coupled to the magnetic alignment of a FM layer [16]. Another way to obtain the magnetically sensitive LPE was demonstrated by Zhou et al. in the Cu/SiO_2/n-Si nonmagnetic system [17]. Using optical injection, the authors achieved a LPV magnetic sensitivity of up to 520 mV T^{-1}. Such a relation between magnetism and the LPE provides the basis for creating LPE-based spintronic and magneto-optical devices, making it possible to control the electronic and magnetic properties of MIS systems via optical means and vice versa. The aforementioned and other studies are primarily focused on investigating the LPE at room temperature. However, in order to search for new photoelectric effects and ways to control them, as well as to gain a deeper understanding of the physical mechanisms responsible for generating LPV, it is important to utilize a wide temperature range. Furthermore, low-temperature effects expand the application of silicon devices, for example, in cryoelectronics [18,19] and aerospace

* Corresponding author. Kirensky Institute of Physics, Federal Research Center KSC SB RAS, Krasnoyarsk, 660036, Russia.
** Corresponding author. Siberian Federal University, Institute of Engineering Physics and Radio Electronics, Krasnoyarsk, 660041, Russia.
E-mail addresses: bia@iph.krasn.ru (I.A. Bondarev), taras@iph.krasn.ru (A.S. Tarasov).

https://doi.org/10.1016/j.mssp.2023.107786
Received 17 April 2023; Received in revised form 1 August 2023; Accepted 2 August 2023
Available online 10 August 2023
1369-8001/

applications [20].

In this work, the lateral photovoltaic effect in Fe/SiO_2/*p*-Si and Mn/SiO_2/*n*-Si structures was studied. Having different types of magnetic ordering, Fe and Mn are compatible with silicon technology and can be deposited as thin films onto silicon substrates using various deposition techniques. Such hybrid structure compositions allow integrating magnetic materials into standard silicon-based electronic devices, making it easier to incorporate magnetic functionality into existing technology. Previously, we have investigated the photovoltaic effect in similar structures [21,22] and have made noteworthy observations regarding the spectral and temperature characteristics of LPE, as well as its response to a magnetic field. The purpose of this current study is to expand upon the previous investigations and perform a comparative analysis of LPE in Fe/SiO_2/*p*-Si and Mn/SiO_2/*n*-Si structures.

2. Experimental details

Samples for investigations were fabricated on silicon substrates. For the Fe/SiO_2/*p*-Si structure, it was a boron doped *p*-Si substrate (the doping density is $p \propto 10^{15}$ 1/cm^3) and for Mn/SiO_2/*n*-Si, phosphorus doped *n*-Si (the doping density is $n \propto 10^{15}$ 1/cm^3). The substrates' surfaces were precleaned using the Shiraki method [23]. In order to form 1.5-nm-thick SiO_2 layers, the corresponding substrates were kept in an aqueous solution of H_2O_2 and NH_4OH (a ratio of 1:1:1) for 30 min at 60 °C. Fe and Mn films were obtained by molecular beam epitaxy (MBE) on an Angara setup [24] using thermal evaporation in ultrahigh vacuum at a rate of 0.25 nm/min. The base pressure in a working chamber was 8.6×10^{-6} Pa. The thicknesses of the obtained films were 5 and 15 nm for Fe and Mn, respectively. Cross-sectional transmission electron microscopy (TEM) images of the samples are presented in Fig. 1.

Fig. 2 shows schematics of the experiment. When the light source illuminates the structure (Fig. 2a), electron-hole pairs are induced in the space charge region of silicon. These pairs get vertically separated in a built-in electric field of the Schottky barrier and, after that, diffuse in the lateral direction, thereby creating a potential difference between the contacts, i.e., the photovoltage. In the present work, we discuss the lateral photovoltage measured on the substrate backside (contacts A(+) and B(−) in Fig. 2b).

The photovoltaic properties were investigated using an experimental setup consisting of a helium cryostat capable of maintaining temperatures between 4.2 K and 300 K, an electromagnet providing a magnetic field range of −1 T–1 T. The photovoltage was measured using a KEITHLEY-2182a nanovoltmeter. The top contacts connecting to the metallic film were created using silver epoxy, while the bottom contacts connecting to the substrate backside were formed by alloying indium.

To conduct optical irradiation, a narrow ~ 0.5 mm strip on the films' surface (Fig. 2b) was specifically targeted. Throughout the entire measurement period, the position of the narrow continuous light beam remained fixed on the surface, positioned asymmetrically relative to the contacts. The source of optical radiation was a halogen lamp with prismatic monochromator, capable of tuning the light wavelength within the range of 0.4–3 μm. In addition, lasers, with wavelengths of 668 nm and 975 nm were utilized. The lasers have adjustable working powers ranging from 0.01 to 500 mW. The external magnetic field *B* was applied in the structure plane, i.e., parallel to the lateral photovoltage (Fig. 2a).

3. Results and discussion

Firstly, let us consider the spectral behavior of the lateral photovoltaic effect. Fig. 3 shows the dependence of the LPV value on the radiation wavelength measured on the substrate backside. The LPV is normalized to the radiation power. The LPV in Fe/SiO_2/*p*-Si and Mn/SiO_2/*n*-Si is hereinafter referred to as LPV_{Fe} and LPV_{Mn}, respectively. Comparing the LPV at $\lambda \leq 750$ nm (inset in Fig. 3), one can see an almost bell-shaped signal followed by an increase in the LPV_{Fe} and a decrease in the LPV_{Mn}. Then, there are the LPV_{Fe} (λ) and LPV_{Mn} (λ) maxima at $\lambda \approx$ 960 nm at $\lambda \approx 1000$ nm, respectively, and the LPV_{Mn} (λ) maximum has a negative sign. In the LPV_{Fe} *(λ)* curve, two peaks with maxima around λ = 960 and 700 nm can be distinguished, which overlap above 700 nm. A similar situation is observed for the $LPV_{Mn}(\lambda)$ curve, but with the overlapping peaks of different signs.

The observed LPV_{Mn} values are significantly lower than the LPV_{Fe} values (Fig. 3). Although LPV_{Mn} and LPV_{Fe} were measured at different temperatures (28.5 and 40 K, respectively), LPV_{Mn} is lower than LPV_{Fe} in the temperature range of 5–45 K, which will be shown below. Such a difference can be explained by three factors. The first one is the thicker Mn film (15 nm) compared to the Fe one (5 nm). As shown in Ref. [2], the LPE sensitivity decreases abruptly as the film thickness increases beyond a certain optimal point. The second factor is the different Schottky barrier heights for Fe/Si and Mn/Si due to the different work functions of Fe (4.67 eV) and Mn (4.10 eV). According to Fowler's theory [25], the photoelectric response R depends on the barrier height φ_B as follows:

$$R \sim (h\nu - q\varphi_B)^2$$

Therefore, different compositions of the structures should result in different LPV values. The third factor is the variation in the type of majority carriers in Si substrates. In Ref. [4], it was reported that the *p*-Si-based MIS structures can exhibit the LPV values almost five times larger than those for the *n*-Si-based structures. The reason for such a difference lies in the electron-hole pair separation mechanism he mechanism of electron-hole pairs' separation was discussed in more detail by Huang et al. in Ref. [4].

In view of the aforesaid, we can assume that the relatively thick Mn film in the Mn/SiO_2/*n*-Si structure, as well as a decrease in the build-in electric field of the MIS structure under illumination lead to the suppression of the LPV. As for the low-wavelength peak observed in both

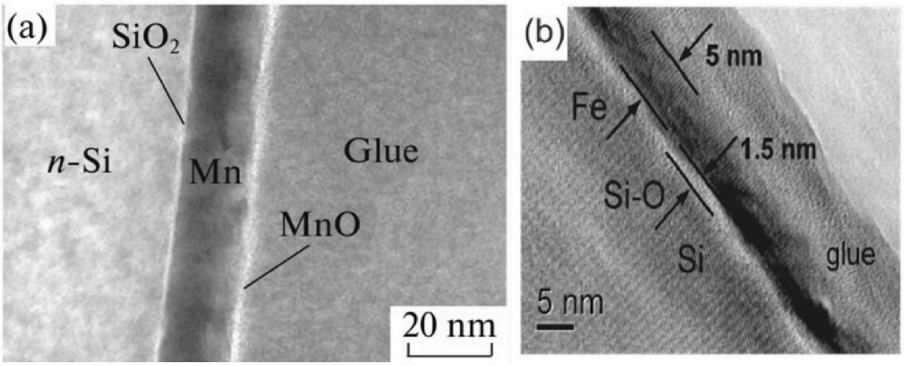

Fig. 1. Cross-sectional transmission electron microscopy (TEM) images of (a) the Mn/SiO_2/*n*-Si (b) Fe/SiO_2/*p*-Si structures.

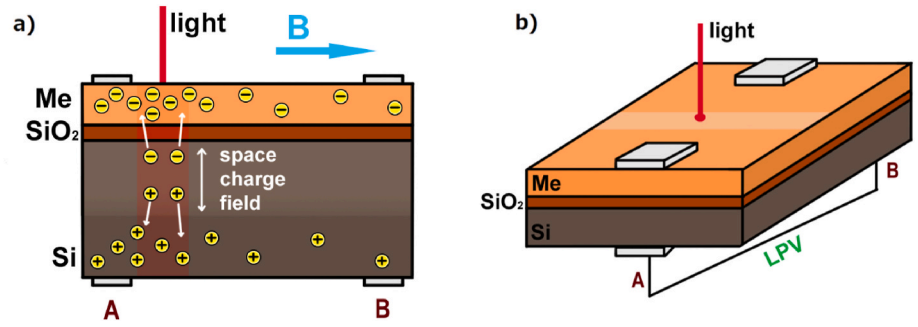

Fig. 2. Schematics of the experiment. (a) Front view and (b) isometric view.

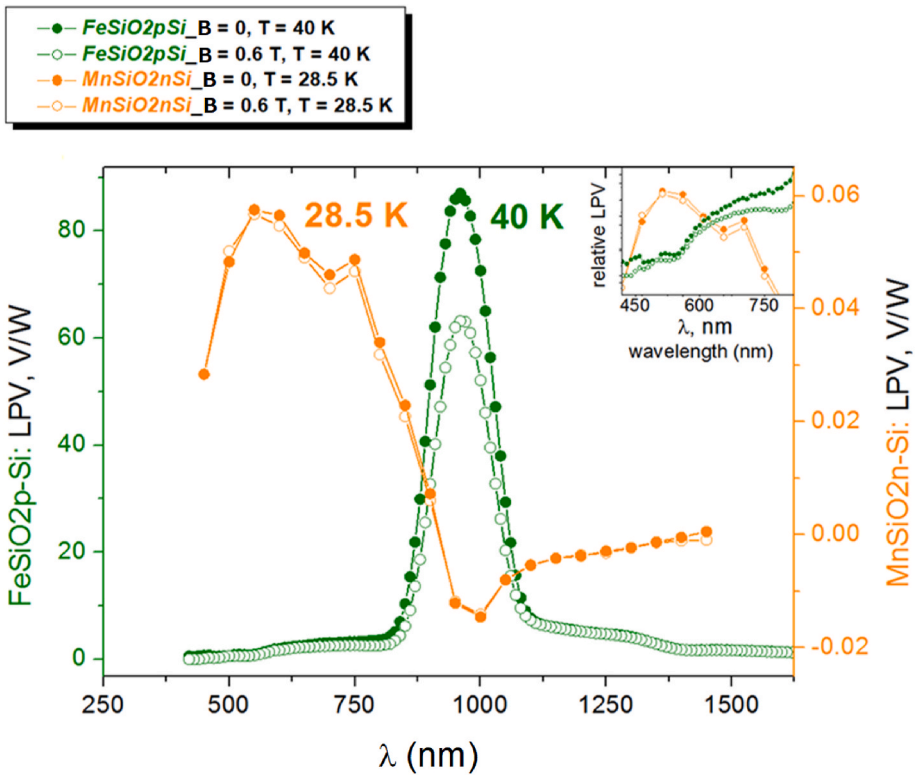

Fig. 3. Wavelength dependences of the LPV for the Fe/SiO_2/*p*-Si (green) and Mn/SiO_2/*n*-Si (orange) structures with $B = 0$ (closed circles) and $B = 0.6$ T (open circles). The inset shows a comparison of the signal shapes in the low-wavelength region ($\lambda < 800$ nm).

the Mn/SiO_2/*n*-Si and Fe/SiO_2/*p*-Si structures, it is most likely related to the absorption in the metallic films caused by electronic transitions, i.e., the Mn and Fe atomic spectra. Since they are next to each other in the periodic table, similar electronic transitions might occur in the λ range of 600–750 nm. Both elements undergo several optical transitions in the λ range of 600–750 nm [26]. The change of sign in the LPV_{Mn} (λ) curve is probably related to the difference in the photon absorption depths. Photons with the low wavelength are absorbed near the Si/SiO_2 interface, while at higher wavelengths they will be absorbed deeper inside the silicon substrate. This will affect the depth of the electron-hole pairs' generation; therefore, their separation and recombination processes will be different. This may lead to a situation when the photovoltaic effect will be determined by carriers of different types, depending on the absorption depth.

Fig. 4 shows the comparison of the $|LPV_{Fe}|$ and $|LPV_{Mn}|$ dependences on the radiation power in the low-temperature region (20–21.5 K). The measurements were performed using a red laser with $\lambda = 668$ nm. The observed LPV growth with increasing power was expected, since the larger number of absorbed photons induces more electron-hole pairs, which contribute to the LPV. It may also be noticed that the LPV_{Fe} (P) curve presumably tends to saturate when the P value exceeds 250 mW. In Ref. [22], we observed that an increase in the radiation power leads to the straightening of the energy bands in silicon, resulting in a decrease in the built-in electric field in the space charge region, preventing some of the photogenerated electron-hole pairs from separating and contributing to the LPV. It seems that, at high powers ($P > 100$ mW), the band straightening surpasses a certain critical point, reducing the number of carriers involved in the LPV and thereby compensating the additional carriers caused by the power growth. It is not completely clear, however, that the LPV would not increase upon the further increase of P.

The temperature dependences of the LPV are presented in Fig. 5a. Comparing the $LPV_{Fe}(T)$ ($P = 1.5$ mW) and $LPV_{Mn}(T)$ ($P = 500$ mW) curves for the two samples, one can see that their shapes are mostly similar. Each curve starts with the negative LPV; then, at $T > 15$ K, the LPV becomes positive and we can see low-temperature peaks (17–20 K) with the more pronounced one for Mn/SiO_2/*n*-Si. At $T \approx 30$ K, the second LPV maxima are observed; here, they can be seen more clearly for Fe/SiO_2/*p*-Si. With a further increase in temperature, the LPV

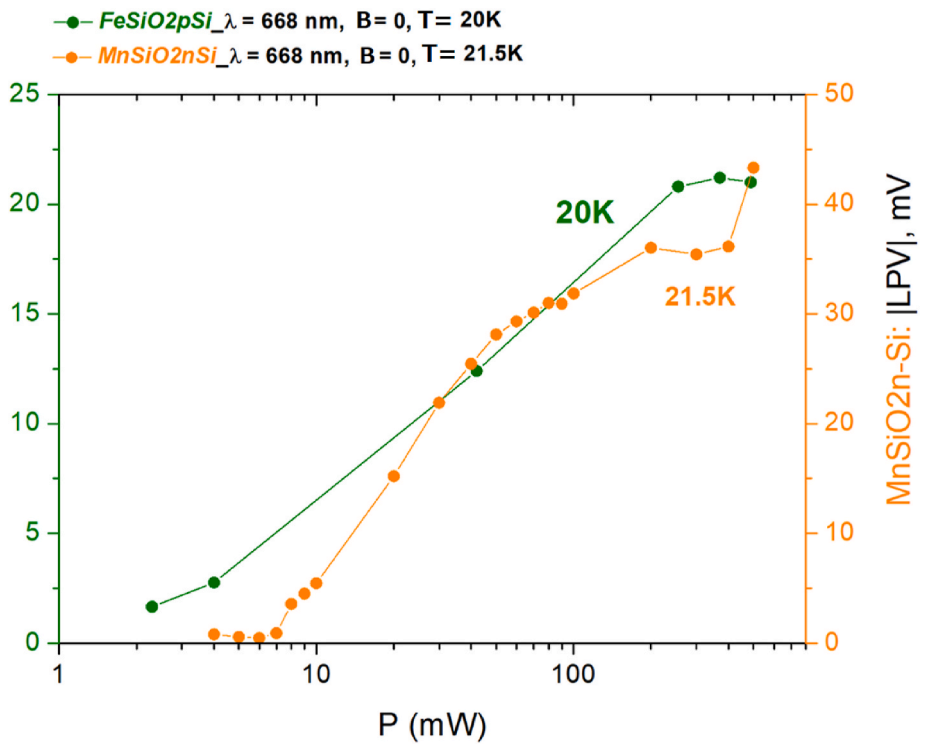

Fig. 4. Dependences of the LPV on the radiation power for Fe/SiO_2/*p*-Si (green) at $T = 20$ K and Mn/SiO_2/*n*-Si (orange) at $T = 21.5$ K on the logarithmic scale. The incoming light wavelength is $\lambda = 668$ nm.

decreases slowly for both samples. The external magnetic field leads to a decrease in the LPV in both cases, except for the narrow temperature region of 26–32 K for Mn/SiO_2/*n*-Si. Fig. 5b shows a relative change in the photovoltage under the action of the magnetic field, which is expressed as

$$MLPV = \frac{LPV(B) - LPV(0)}{\mathrm{LPV}(0)} \bullet 100\% \quad (1)$$

Previously, we reported on the low-temperature behavior of the LPV in the Mn/SiO_2/*n*-Si structure [22]. We attributed the low-temperature magnetic field-dependent LPV peak to the surface states, which are located near the SiO_2/Si interface of the structure. These surface states were observed in a number of different MIS structures [27–29]. Supposedly, in the low-temperature range, the Fermi level in silicon crosses these interface energy levels, which makes them deionized and initiates the electron (hole) excitation and transition from the interface centers into the conduction (valence) band of silicon under illumination. The additional carrier generation channel results in the growth of the LPV. Due to the absorption of light by the interface centers, the emitted electrons possess high kinetic energy. We called these electrons "hot". These electrons are expected to exhibit high diffusion velocity, enabling them to diffuse radial direction with minimal recombination. This diffusion process results in an elevated carrier concentration, primarily near the illumination point (contact A in Fig. 2a). Consequently, the difference in carrier densities between contacts A and B becomes more pronounced, leading to a larger LPV. The magnetic field changes the hot electron emission process, decreasing the LPV. Additionally, it is noteworthy that there are actually two $\mathrm{LPV_{Mn}}(T)$ peaks in the T range of 15–25 K (Fig. 5a), which can be seen more clearly under the effect of the magnetic field.

With a further decrease in temperature, the majority carrier density drops, leading to an increase in the space charge region width and, consequently, to a decrease in the Schottky field. As a result, the efficiency of photogenerated hole-electron separation lowers and the LPV decreases. At some point, the Schottky field almost disappears, so it is safe to assume that the LPV measured below 20 K is produced by a different mechanism.

The inset to Fig. 5a shows the $\mathrm{LPV_{Mn}}(T)$ curve at $P = 1.5$ mW. As we can see, the maximum $\mathrm{LPV_{Mn}}$ value only slightly exceeds −2 mV, whereas $\mathrm{LPV_{Fe}}(T)$ attains almost 45 mV. Earlier, we explained the difference in the signal amplitudes. Interestingly, the LPV peak changes its sign. The temperature of the $\mathrm{LPV_{Mn}}(T)_{P\,=\,1.5mW}$ peak corresponds to the second of $\mathrm{LPV_{Mn}}(T)_{P\,=\,500mW}$ peak, which can be seen under the effect of the magnetic field. In light of the above, we can conclude that, in the $\mathrm{LPV_{Mn}}(T)_{P\,=\,500mW}$ curve, two peaks are hidden in one: one of them, with lower T, corresponds to hot electrons and the second one can be related to the $\mathrm{LPV_{Fe}}(T)_{P\,=\,1.5mW}$ peak at 18 K and be caused by other impurity states in Si.

The magnetic field affects the LPV via two mechanisms. The first one is the action of the Lorentz force, which deflects the photogenerated carriers' trajectories, resulting in the lower LPV. The second mechanism is shifting or splitting of the interface state levels E_s in magnetic field that schematically shown on Figs.6a, b, which redistributes these states and changes contribution to the photovoltage. In the low-temperature region, the surface centers play an active role in the LPE because they become deionized. This allows them to participate in carrier photogeneration and reduces their role in recombination. Therefore, their shifting by a magnetic field leads to changes in their position relative to E_F and, consequently, ionization/deionization depending on the specific temperature. This results in the emergence of the MLPV effect. Experimental observations of change in energy of levels located within the band gap have been made using various methods in p-doped and n-doped Si [30] and n-type GaAs. [31]. Significant changes in dark current, as well as magnetoresistance and magnetoimpedance effects, have been observed in such structures [27–29]. It is logical to assume that in similar structures and within a close temperature range, magnetic field also influences the photovoltage through this mechanism. However, the physical mechanism is still not fully understood, mainly due to the significant increase in energy of levels in a magnetic field, on the order of a few meV at a magnetic field of 1T. It is more likely that the main

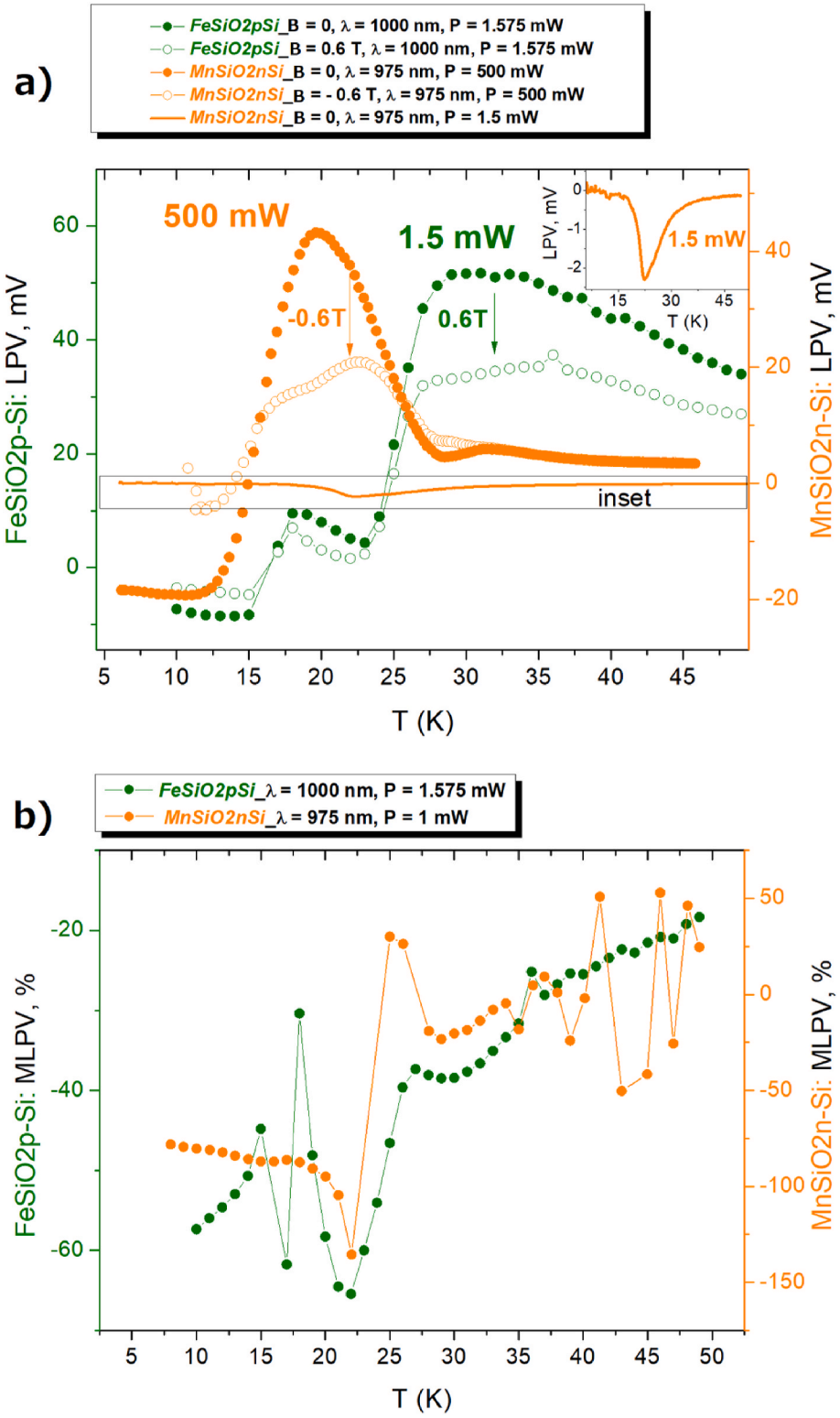

Fig. 5. (a) Temperature dependences of the LPV for Fe/SiO_2/*p*-Si (green) at $P = 1.5$ mW and Mn/SiO_2/*n*-Si (orange) at $P = 500$ mW in $B = 0$ (closed circles) and in external magnetic fields (open circles). The inset shows the $LPV_{Mn}(T)$ curve at $P = 1.5$ mW. (b) Temperature dependences of MLPV for the same structures.

mechanism is enhanced Zeeman splitting [32]. The increase in shifting or splitting can be attributed to (i) the exchange interaction between *s* and *p* electrons in surface states and *d* electrons in the electrode near the interface, and (ii) an electric field in the space charge region. The non-monotonic behavior of MLPV with temperature variation is associated with both the competition of magnetic field influences and possibly its different effects on electrons and holes. It is noteworthy that the MLPV value is positive around 28 K (Fig. 5b), which means that the magnetic field increases the LPV. If we assume that the corresponding $LPV_{Mn}(T)_{P\ =\ 500mW}$ minimum (Fig. 5a) is related to the negative contribution of minority carriers (holes), the magnetic field will suppress this contribution as well, thereby increasing the LPV.

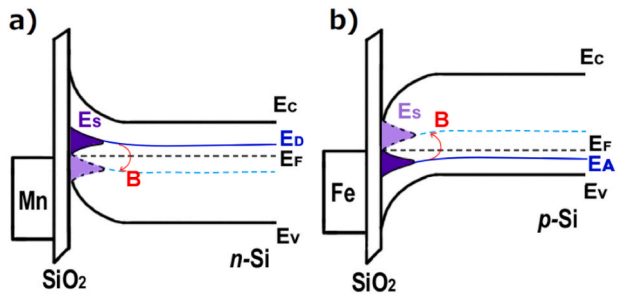

Fig. 6. Shifting of the interface states in magnetic field for (a) the Mn/SiO_2/*n*-Si and (b) Fe/SiO_2/*p*-Si structures. E_D and E_A are the bulk donor and acceptor states, respectively. E_S represents the interface states located within the space charge region.

4. Conclusions

The lateral photovoltaic effect in the Fe/SiO_2/*p*-Si and Mn/SiO_2/*n*-Si hybrid structures was studied. It was found that the LPV(λ) curve for each sample contains two maxima (two overlapping peaks for LPV(λ)$_{Fe}$ and positive and negative maxima for LPV(λ)$_{Mn}$). The lower amplitude of LPV_{Mn} compared to LPV_{Fe} is mainly caused by the strong light absorption in the 15-nm Mn film due to its large thickness and also due to the difference in Schottky barrier in Fe/*p*-Si and Mn/n-Si structures. The low-wavelength maxima in the $LPV_{Fe}(\lambda)$ and $LPV_{Mn}(\lambda)$ curves are most likely related to the atomic absorption in Fe and Mn. The power dependences of the LPV revealed that the LPV reaches saturation at $P >$ 250 mW. The temperature dependences of the LPV showed that, above 30 K, the LPV slowly decreases with an increase in temperature. Below 30 K, transport of photogenerated carriers is strongly affected by the surface states located near the SiO_2/Si interface, which cause the drastic rise of the LPV_{Mn} around 20 K. This rise is induced by emission of "hot" electrons. These electrons possess high kinetic energy, and their involvement in the diffusion process leads to an increased carrier concentration, predominantly in the vicinity of the illuminated area, increasing an asymmetry of the carriers' distribution. Below 20 K, the electric field in the space charge region responsible for separation of photogenerated carriers is suppressed and the LPV is governed by other mechanisms. The magnetic field affects the LPV in two ways: by deflecting the trajectories of photogenerated carriers and by shifting of the interface state energy levels. It was experimentally demonstrated that the choice of a semiconductor material for a MIS structure is essential for the LPE. As for a metallic film, its effect on the LPV is apparently more related to the film thickness than to the metal type. Some low-temperature features of the LPE and the ways to affect it by substrate impurities and an external magnetic field were demonstrated. The results obtained can be used to deepen our understanding of the peculiarities of the LPE in silicon-based structures and, in particular, the role of the SiO_2/Si interface in photogenerated transport.

CRediT authorship contribution statement

I.A. Bondarev: Writing – review & editing, Writing – original draft, Investigation. **M.V. Rautskii:** Writing – review & editing, Supervision, Investigation. **N.V. Volkov:** Supervision, Conceptualization. **A.V. Lukyanenko:** Investigation. **I.A. Yakovlev:** Investigation. **S.N. Varnakov:** Investigation. **A.S. Tarasov:** Writing – review & editing, Validation, Supervision.

Declaration of competing interest

The authors declare that they have no known competing financial interests or personal relationships that could have appeared to influence the work reported in this paper.

Data availability

Data will be made available on request.

References

[1] M.N. Baibich, J.M. Broto, A. Fert, F. Nguyen, V.D. Dau, F. Petroff, P. Etienne, G. Creuzet, A. Friederich, J. Chazelas, Phys. Rev. Lett. 61 (1988) 2472.
[2] C. Yu, i, H. Wang, Sensors 10 (2010) 10155–10180.
[3] H. Wang, S.Q. Xiao, C.Q. Yu, Y.X. Xia, Q.Y. Jin, Z.H. Wang, New J. Phys. 10 (2008), 093006.
[4] X. Huang, C. Mei, J. Hu, D. Zheng, Z. Gan, P. Zhou, H. Wang, IEEE Electron. Device Lett. 37 (2016) 1018–1021.
[5] A. Dong, H. Wang, Ann. Phys. 531 (2019), 1800440.
[6] W. Schottky, Z. Phys. 31 (1930) 913.
[7] J.T. Wallmark, Proc. IRE 45 (1957) 474.
[8] C.Q. Yu, H. Wang, Appl. Phys. Lett. 96 (2010), 171102.
[9] S. Liu, X. Xie, H. Wang, Opt Express 22 (2014), 11627.
[10] C. Yu, H. Wang, Sensors 10 (2010), 10155.
[11] I. Martinez, J.P. Cascales, A. Lara, P. Andres, F.G. Aliev, AIP Adv. 5 (2015), 117207.
[12] H. Wang, S.Q. Xiao, C.Q. Yu, Y.X. Xia, Q.Y. Jin, Z.H. Wang, New J. Phys. 10 (2008), 093006.
[13] S.Q. Xiao, H. Wang, Z.C. Zhao, Y.X. Xia, Z.H. Wang, J. Phys. D Appl. Phys. 41 (2008), 045005.
[14] L.Z. Kong, H. Wang, S.Q. Xiao, J.J. Lu, Y.X. Xia, G.J. Hu, N. Dai, Z.H. Wang, J. Phys. D Appl. Phys. 41 (2008), 052003.
[15] J. Hu, Q. Zhang, P. Zhou, C. Mei, X. Huang, A. Dong, D. Zheng, H. Wang, IEEE Photon. Technol. Lett. 29 (2017) 1848.
[16] S. Wang, W. Wang, L. Zou, X. Zhang, J. Cai, Z. Sun, B. Shen, J. Sun, Adv. Mater. 26 (2014) 8059.
[17] P. Zhou, Z. Gan, X. Huang, C. Mei, Y. Xia, H. Wang, Sci. Rep. 7 (2017), 46377.
[18] I. Kochanek, Nucl. Instrum. Methods Phys. 980 (2020), 164487.
[19] M. D'Incecco, C. Galbiati, G.K. Giovanetti, G. Korga, X. Li, A. Mandarano, A. Razeto, D. Sablone, C. Savarese, IEEE Trans. Nucl. Sci. 65 (2017) 591–596.
[20] R.L. Patterson, A. Hammoud, M. Elbuluk, 12th International Components for Military and Space Electronics Conference, CMSE 08, 2008. No. E-16851.
[21] N.V. Volkov, M.V. Rautskii, A.S. Tarasov, I.A. Yakovlev, I.A. Bondarev, A. V. Lukyanenko, S.N. Varnakov, S.G. Ovchinnikov, Phys. E: Low-Dimens. 101 (2018) 201–207.
[22] I.A. Bondarev, M.V. Rautskii, I.A. Yakovlev, M.N. Volochaev, A.V. Lukyanenko, A. S. Tarasov, N.V. Volkov, J. Semiconduct. 53 (2019) 1954–1958.
[23] A. Ishizaka, Y. Shiraki, J. Electrochem. Soc. 133 (1986) 666.
[24] S.N. Varnakov, A.A. Lepeshev, S.G. Ovchinnikov, A.S. Parshin, M.M. Korshunov, P. Nevoral, Instrum. Exp. Tech. 47 (2004) 839.
[25] R.H. Fowler, Phys. Rev. 38 (1931) 45.
[26] A. Kramida, Y. Ralchenko, J. Reader, NIST ASD Team, NIST Atomic Spectra Database (ver. 5.1), National Institute of Standards and Technology, Gaithersburg, MD, 2013.
[27] J.J.H.M. Schoonus, F.L. Bloom, W. Wagemans, H.J.M. Swagten, B. Koopmans, Phys. Rev. Lett. 100 (2008), 127202.
[28] N.V. Volkov, A.S. Tarasov, D.A. Smolyakov, A.O. Gustaitsev, V.V. Balashev, V. V. Korobtsov, Appl. Phys. Lett. 104 (2014), 222406.
[29] N.V. Volkov, A.S. Tarasov, D.A. Smolyakov, A.O. Gustaitsev, M.V. Rautskii, A. V. Lukyanenko, M.N. Volochaev, S.N. Varnakov, I.A. Yakovlev, S.G. Ovchinnikov, AIP Adv. 7 (2017), 015206.
[30] D.A. Smolyakov, A.S. Tarasov, I.A. Yakovlev, A.N. Masyugin, M.N. Volochaev, I. A. Bondarev, N.N. Kosyrev, N.V. Volkov, Thin Solid Films 671 (2019) 18–21.
[31] T.W. Hickmott, Phys. Rev. B 46 (1992), 12342.
[32] T. Dietl, H. Ohno, Rev. Mod. Phys. 86 (2014) 187.